THE ASTROPHYSICAL JOURNAL, 293:508–521, 1985 June 15

HIGH-VELOCITY GAS FLOWS ASSOCIATED WITH H_2 EMISSION REGIONS: HOW ARE THEY RELATED AND WHAT POWERS THEM?

J. FISCHER,[1,2,3] D. B. SANDERS,[4,5] M. SIMON,[5] AND P. M. SOLOMON[5]

Received 1984 July 30; accepted 1984 December 31

ABSTRACT

We report on an investigation of high-velocity molecular material near the vibrationally excited H_2 emission regions in the objects DR 21, W75 N, NGC 7538, OMC-2, NGC 6334/Peak V, and the Herbig-Haro Object 2. The $^{12}CO(J = 1–0)$ and $^{13}CO(J = 1–0)$ transitions were used as tracers of the high-velocity molecular flows. All the H_2 sources are associated with bipolar CO high-velocity flows. We also present a new high-spatial-resolution map (11″) of the DR 21 H_2 region. The spatial relationship of the high-velocity gas and the vibrationally excited gas, together with the similarity of the energies involved in the two molecular components, is convincing evidence to support the scenario in which the H_2 emission traces the cooling gas that has been shocked by outflowing gas. Although radiation pressure could be responsible for driving the flows in OMC-2 and NGC 7538, it is unlikely to be the driving mechanism in DR 21 and W75 N. Similarly, H II region expansion does not appear to be the driving mechanism for any of the outflows.

Subject headings: interstellar: molecules — stars: pre–main-sequence

I. INTRODUCTION

Essential to our understanding of both the evolution of protostars during their approach onto the main sequence and of the molecular clouds from which they are formed is the study of the interaction between these two entities. Within the past decade, infrared and millimeter observations of molecular emission in regions of star formation have led to the discovery of extremely energetic expanding flows that may be intimately related to the star-formation process as well as the lifetimes and structure of molecular clouds. In this paper, we describe our study of the high-velocity gas flows, using observations of the CO ($J = 1–0$) line as a tracer, in the molecular-cloud regions in which we have previously detected vibrationally excited 2 μm H_2 line emission, i.e., in DR 21, W75 N, OMC-2, Herbig-Haro object 2, NGC 7538, and NGC 6334 (Fischer, Righini-Cohen, and Simon 1980; Gautier 1978; Fischer *et al.* 1980; Fischer *et al.* 1982).

Of the possible ways of producing vibrationally excited H_2 within molecular clouds (see Shull and Beckwith 1982 for review), thermal excitation by shocks formed in high-velocity flows seems the most plausible. Analysis of the observed H_2 line strengths for the Orion, DR 21, and OMC-2 sources rules out pure ultraviolet excitation (Gautier *et al.* 1976; Fischer, Righini-Cohen, and Simon 1980; Thronson and Thompson 1982). Velocity-resolved profiles of the H_2 emission lines of Orion and NGC 2071 show that the line emission is formed in high-velocity flow regions, and a close association is observed in the Orion source between the H_2 emission region and the gaseous component of the molecular cloud that is flowing at high velocity (Nadeau, Geballe, and Neugebauer 1982; Persson *et al.* 1981; Solomon, Huguenin, and Scoville 1981). There is much additional evidence to support the belief that the high-velocity gas flows that are observed in molecular-cloud cores are due to expansion (Lada and Harvey 1981; Bally and Lada 1983).

The conjecture that the high-velocity flows within molecular clouds and the H_2 emission regions are related is thus a natural one. This idea has been the basis of search strategies for H_2 emission (Bally and Lane 1982; Simon and Joyce 1983) and has yielded the discovery of a number of H_2 emission regions. However, the presence of CO high-velocity outflows has by no means been 100% successful as a predictor of detectable H_2 emission. This may be attributed to the fact that the H_2 emission is extremely sensitive to the gas temperature and density and to obscuration by dust. Thus, in order to investigate the connection between the outflows and the shocked H_2, in this work we investigate the inverse question: are high-velocity flows that are detectable via their CO emission present in all vibrationally excited H_2 sources? The CO 2.6 mm emission does not suffer extinction due to dust and is not as sensitive to temperature and density. Therefore, this search strategy should prove to be nearly 100% successful if indeed molecular high-velocity outflows are responsible for most H_2 emission regions. In this work our goals are (1) to determine whether there is a physical association between the H_2 emission and high velocity flow regions (2) to investigate whether the high-velocity flows can power the H_2 emission, and (3) to investigate whether radiation pressure or H II region expansion can drive the outflows. We use the ^{12}CO and ^{13}CO profiles to determine the spatial extent, optical depth, column density, momentum, and energy of the outflows.

II. OBSERVATIONS

Radio spectroscopic observations of the $J = 1–0$ line emission of ^{12}CO and ^{13}CO were obtained with the 11 m telescope of the NRAO[6] and the 14 m telescope of the Five College

[1] E. O. Hulburt Center for Space Research, Naval Research Laboratory.
[2] Visiting Astronomer, Kitt Peak National Observatory, operated by the Association of Universities for Research in Astronomy, Inc., under contract with the National Science Foundation.
[3] NRC-NRL Cooperative Research Associate.
[4] Five College Radio Astronomy Observatory, University of Massachusetts, Amherst.
[5] Astronomy Program, State University of New York at Stony Brook.

[6] The National Radio Astronomy Observatory is operated by Associated Universities, Inc., under contract with the National Science Foundation.

TABLE 1

JOURNAL OF CO OBSERVATIONS

	NRAO		FCRAO	
SOURCE	$^{12}CO(J = 1–0)$	$^{13}CO(J = 1–0)$	$^{12}CO(J = 1–0)$	$^{13}CO(J = 1–0)$
DR 21	1980 June	1982 Apr	...	...
W75 N	1982 Apr	...	1984 May	1984 May
NGC 7538	...	...	1984 May	1982 Dec
OMC-2	...	...	1980 Mar, 1982 Dec	1982 Dec
NGC 6334	1980 June, 1982 Apr	1982 Apr	...	...
HH 2	...	...	1980 Mar	...

Radio Astronomy Observatory (FCRAO)[7]. Table 1 gives the journal of the observations. At 2.6 mm, the beam sizes are 66″ and 44″ (FWHP) at NRAO and FCRAO respectively. At NRAO, a cooled dual-channel mixer receiver was used. The signal in each receiver polarization channel was analyzed with two parallel banks of 128 filters of 250 kHz and 500 kHz resolution. At FCRAO, a cooled mixer receiver was used and the signal was analyzed with 256 filters 250 kHz wide. A rotating chopper wheel was used to calibrate the data. All the observations were carried out in the position-switching mode. The telescope pointing was checked by continuum observations of the planets and DR 21. The pointing accuracy of the NRAO and FCRAO antennae was ±15″ and ±7″ respectively. All line temperatures T_A* presented in this paper have been corrected for the effects of the Earth's atmosphere, ambient temperature telescope losses, and subreflector spillover. The additional correction that accounts for the main beam coupling efficiency η is discussed in the analysis section.

The new 11″ resolution observations of the $S(1)$ $v = 1–0$ line emission of DR 21/H_2 were obtained with a cooled, InSb-equipped, circular variable-filter spectrometer (spectral resolution $\lambda/\Delta\lambda = 77$) at the 1.3 m telescope of the Kitt Peak National Observatory in 1980 September and November. Data were taken with an 11.″3 beam at angular intervals of 10″, and the signal–reference beam separation was generally 90″ north-south. Wavelength calibration was checked by observations of the Bγ line of NGC 7027, and flux calibration was based on interpolation of broad-band photometry of ϵ Cyg.

III. OBSERVATIONAL RESULTS

a) DR 21

Strong emission of vibrationally excited H_2 is found ~1′ to the east of the compact H II region DR 21, with a diameter of ~1′ (Fischer, Righini-Cohen, and Simon 1980). Although the H_2 emission region is well away from the association of free-free emission condensations that make up DR 21 (see Harris 1973 for a high-resolution map), diffuse Bγ line emission is present at several positions in the H_2 source (Fischer, Righini-Cohen, and Simon 1980). This Bγ radiation is probably associated with the faint extension of the DR 21 H II region reported by Ryle and Downes (1967) and Wynn-Williams (1971). Weaker $S(1)$ line emission is also found at the position of W75 IRS 1 in this cloud (Fischer, Righini-Cohen, and Simon 1980).

To improve our knowledge of the structure of the DR 21 H_2 emission region, and thus to try to identify the source driving the H_2 emission, we remapped it in the $v = 1–0$ $S(1)$ line at 11″ resolution (Fig. 1). At this resolution, the H_2 line emission is remarkably smoothly distributed and peaks 75″ to the east of the H II region component D identified by Harris (1973).

Dickel, Dickel, and Wilson (1978) have found that the DR 21/W75 S and W75 N (approximately 20′ north of DR 21) sources are within two large molecular clouds, at radial velocities of $v_{LSR} = -3$ km s^{-1} and 9 km s^{-1} respectively, and they suggested that the two clouds are interacting. We therefore adopt one distance, 2 kpc (Dickel, Dickel and Wilson 1978; Cong 1977) for the entire complex.

Evidence for high-velocity gas flow in the molecular cloud associated with DR 21 was first presented by Dickel, Dickel, and Wilson. We present a velocity versus declination map of T_A*(^{12}CO) for DR 21 in Figure 2. The (0, 0) position of this map is at the peak of the 3 mm radio continuum emission of DR 21 as measured with the NRAO telescope. We will refer to this position at R.A.(1950) = $20^h37^m14^s.3$ and decl.(1950) = 42°09′00″ as the radio continuum centroid position. ^{12}CO emission extends to ±28 km s^{-1} of the −3 km s^{-1} component. A map of the intensity of the blue wing, integrated over the velocity range −20 to −10 km s^{-1}, is shown in Figure 3. The DR 21 H_2 emission region is situated at the periphery of the high-velocity molecular flow. We define the measured angular diameter θ (FWHP) in terms of the area within the half-power contour of the integrated intensity: area (FWHP) = $\pi\theta^2$ (FWHP)/4. For the blue-wing emission region of DR 21, θ (FWHP) = 2.′1. The source peaks 25″ ± 15″ west and 25″ ± 15″ south of the DR 21 radio continuum centroid position. We have also measured the position and size of the CO emission between −19 and −16 km s^{-1} and have found that they remain approximately constant for these velocity intervals. The declination-velocity map (Fig. 2) of the ^{12}CO emission shows that there is also high-velocity emission in the red wing of the −3 km s^{-1} component and that the blue- and red-wing emission regions peak at different positions. Because of the strong emission of the W75 N component at +9 km s^{-1}, it is difficult to determine the position and extent of the red-wing emission. Figure 3 shows that there is a local peak in the distribution of the integrated intensity of the 9 km s^{-1} component (integrated between 5 and 20 km s^{-1}) that is located ~1′ north of the DR 21 radio continuum centroid position. If this is interpreted as the contribution from the red wing, then the total positional displacement between the red- and blue-wing emission regions is about 1.′75 (~1 pc).

It is clear from Figures 2 and 3 that the W75 IRS 1 H_2 region lies at the periphery of a secondary peak in the blue wing of the DR 21 (−3 km s^{-1} component) high-velocity flow. This peak appears to be a separate outflow associated with the DR 21 (OH) and the W75 IRS 1 sources. We have chosen not to

[7] The FCRAO is operated by the University of Massachusetts with support from the National Science Foundation under grant AST82-12252 and with the permission of the Metropolitan District Commission.

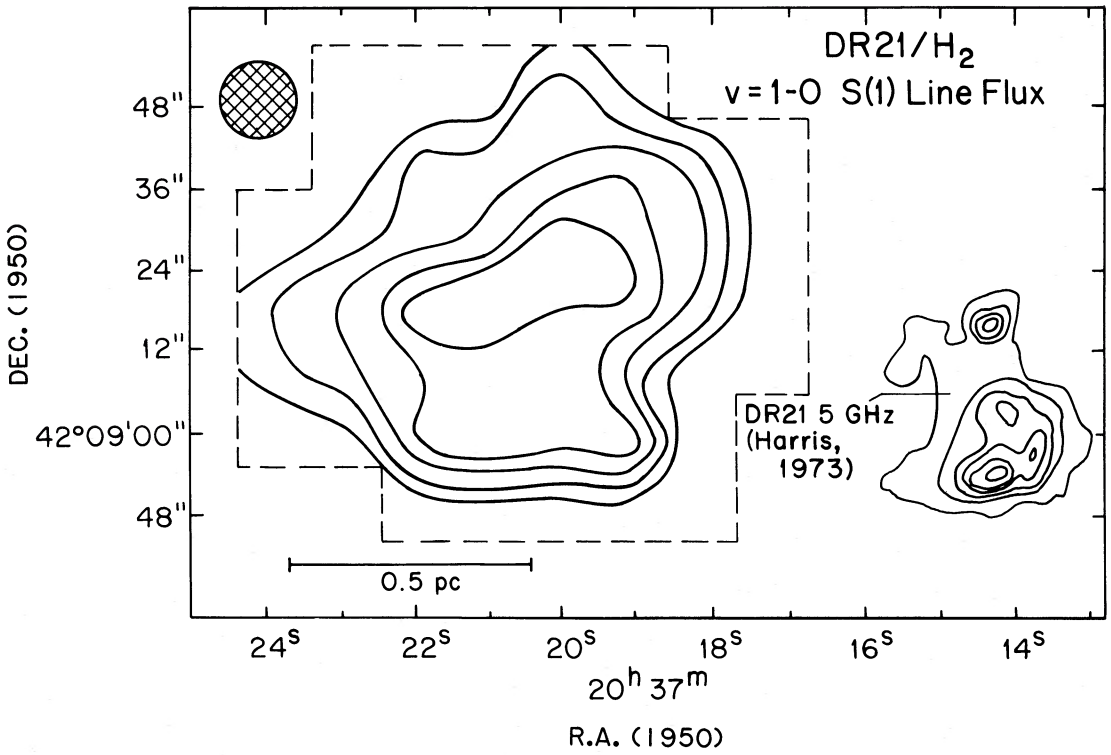

FIG. 1.—Map of the DR 21 H_2 source in the $v = 1$–0 $S(1)$ line at 11″ angular resolution. The first contour intensity level and the intervals are 2×10^{-5} ergs cm^{-2} s^{-1} sr^{-1}. The signal-to-noise ratio for the first contour is 1. The dashed line indicates the limits of the region mapped and the hatched circle shows the beam size. The 5 GHz radio continuum contours, for which the first contour is 392 K and the subsequent intervals are 784 K, were obtained from Harris (1973).

conduct a detailed study of this outflow due to its proximity to the strong DR 21 outflow.

We obtained a high-sensitivity profile of the ^{12}CO line at the centroid position of the DR 21 radio continuum emission (Fig. 2). The ratio $R \equiv T_A^*(^{12}\mathrm{CO})/T_A^*(^{13}\mathrm{CO})$ as a function of velocity averaged in 0.65 km s^{-1} velocity intervals is shown in Figure 2. If both lines were optically thin and if the excitation temperature of the two species is the same, then the ratio of the line intensities would be the same as the species-abundance ratio. Figure 2 shows that the line-temperature ratio is significantly lower than the solar-abundance ratio, $^{12}\mathrm{CO}/^{13}\mathrm{CO} = 90$. The average value of the ratio R in the blue wing is 25 ± 2 (see Table 2), indicating that the high-velocity ^{12}CO is somewhat optically thick (see § IV).

b) W75 N

The W75 N region contains a cluster of compact H II regions (see, e.g., Haschick *et al.* 1981). We assume its distance to be the same as for DR 21, 2 kpc (see § III*a*). Emission in the H_2 $v = 1$–0 $S(1)$ and Q-branch lines was detected by Fischer, Righini-Cohen, and Simon (1980) at a position centered on W75 N(A) although no mapping observations were done. The center of our grid of ^{12}CO observations was also at W75 N(A). A declination-velocity map of $T_A^*(^{12}\mathrm{CO})$ through the peak of the red-wing emission is shown in Figure 4. The strong emission at $v_{\mathrm{LSR}} = 9$ km s^{-1} and -3 km s^{-1} is from the molecular-cloud components associated with W75 N and DR 21 respectively. The strongest high-velocity emission in the ^{12}CO line was found at a position 1′ south and 1′ west of W75 N(A). Line emission at velocities redshifted with respect to the 9 km s^{-1} component is prominent to at least $v_{\mathrm{LSR}} = 27$ km s^{-1}. That this red-wing emission is localized to the W75 N region is clearly shown by the declination versus velocity map and the map of blue- and redshifted ^{12}CO emission shown in Figure 5. It is difficult to investigate the blue-wing component because of the DR 21 line emission centered at $v_{\mathrm{LSR}} = -3$ km s^{-1}. The angular extent of both wings, determined using equal, uncontaminated velocity intervals, is approximately equal: θ (FWHP) = 2′.3 (blue) and 1′.8 (red). The blue and red emission

TABLE 2

OBSERVED PARAMETERS OF HIGH-VELOCITY EMISSION REGIONS

	Blue Wing					Red Wing			
Source	v_0 (km s^{-1})	d_{hv} (pc)	$\lvert v_l - v_0 \rvert$ (km s^{-1})	$\lvert v_h - v_0 \rvert$ (km s^{-1})	R	d_{hv} (pc)	$\lvert v_l - v_0 \rvert$ (km s^{-1})	$\lvert v_h - v_0 \rvert$ (km s^{-1})	R
DR 21	−3	1.06	7	27	25 ± 2	...	...	...	...
W75 N	+9	...	...	...	...	0.95	10	21	24 ± 7
NGC 7538	−57	0.75	8	12	23 ± 2	0.75	11	17	23 ± 5
OMC-2	+10.5	0.23	3.3	7	26 ± 8	0.17	3.3	6	27 ± 7
NGC 6334	−5	0.8	6	18	5.7 ± 0.5	...	...	...	...

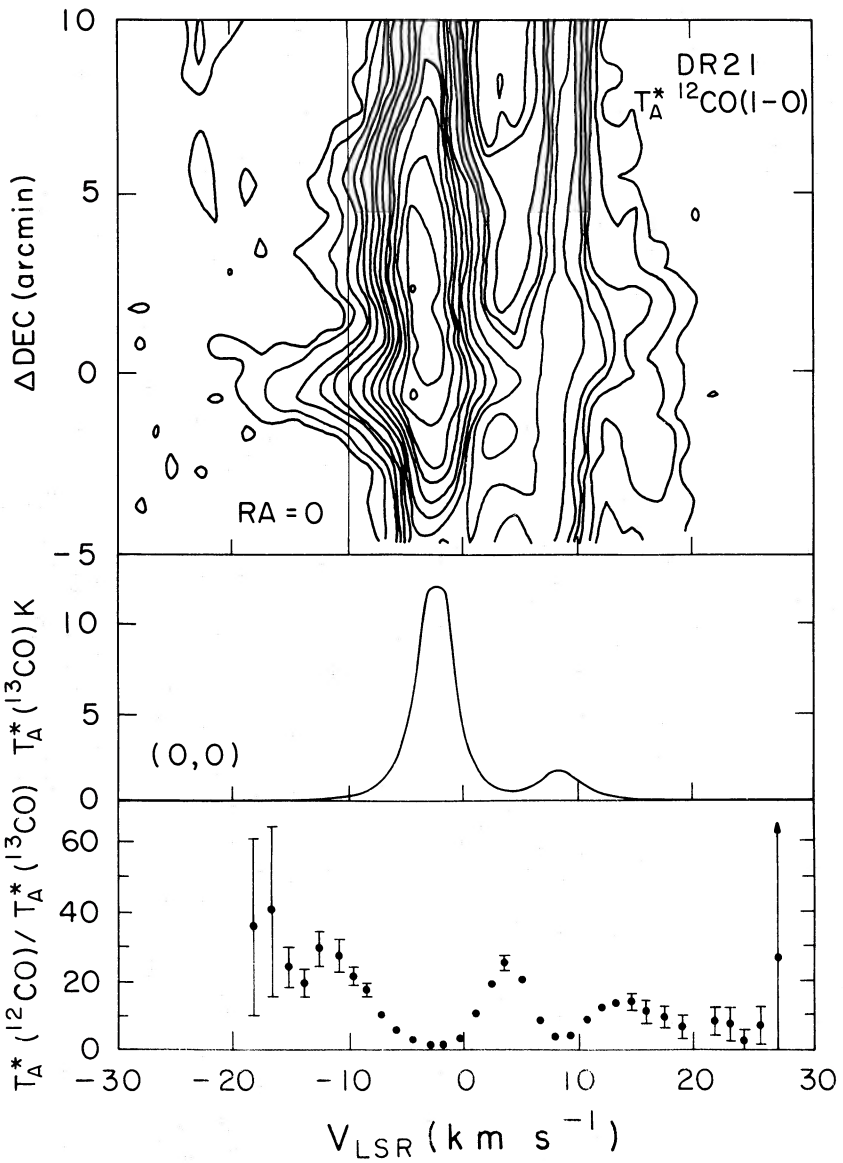

FIG. 2.—(*top*) Velocity-declination map of $T_A^*(^{12}CO)$ $J = 1$–0 for DR 21. The (0, 0) position is at the radio continuum centroid, and thus the right ascension of this strip map is ~ 1′12″ to the west of the H_2 emission peak shown in Fig. 1. The vertical line indicates the value taken for the velocity v_l (see § IV*b*). The ^{12}CO data were taken at 30″ spacing between Δdecl. = ±3′ and otherwise at 1′ spacing. The contour levels are $T_A^* = 0.5, 1, 2, 3, 4, 6, 8, \ldots, 22$ K km s^{-1}. (*middle*) The ^{13}CO ($J = 1$–0) line profile and (*bottom*) the ratio $T_A^*(^{12}CO)/T_A^*(^{13}CO)$ as a function of velocity are shown at the DR 21 radio continuum centroid.

peaks are separated by 1′ (~0.6 pc). The ratio of ^{12}CO to ^{13}CO antenna temperatures, estimated for the uncontaminated red-wing emission by integrating between 20 and 30 km s^{-1}, is 24 ± 7, which suggests that the high-velocity flow associated with W75 N, like DR 21, is optically thick.

c) NGC 7538

Observations of the H_2 $S(1)$ line emission of this region at 34″ resolution showed that the emission peaks at a position between the optically visible H II region NGC 7538 and the cluster of infrared sources IRS 1, 2, and 3 which are strongly obscured by the NGC 7538 molecular cloud (Fischer *et al.* 1980). It was unclear whether the driving agent of the H_2 emission is associated with the visible H II to the north or with the IR cluster to the south. A declination versus velocity map of $T_A^*(^{12}CO)$ through IRS 1 is shown in Figure 6.

The continued velocity broadening 2′ south of IRS 1 is part of a second outflow, one of at least three additional outflows within a 5′ radius of IRS 1–3 (Sanders 1985). Figure 7 shows a spatial map of the blue and red high-velocity gas associated primarily with IRS 1–3. The high-velocity flow is clearly bipolar, with blue and red emission peaks separated by 0′.6, which is about 0.5 pc at the adopted distance of 2.8 kpc (Crampton, Georgelin, and Georgelin 1978). The eastern and southern boundaries of the central outflow are confused with high-velocity emission from nearby sources. Our map, obtained with a 44″ beam, and our interpretation of the NGC 7538 IRS 1–3 high-velocity outflow differs in several ways from recent results presented by Campbell and Thompson (1984), who mapped the NGC 7538 CO outflow with the 66″ beam of the NRAO 36 foot (11 m) telescope. They reported seeing no separation between blue and red emission peaks. They also interpret extended high-velocity emission to the southwest and south as being part of the outflow from IRS 1–3. In addition, their map shows a high-velocity emission peak approximately

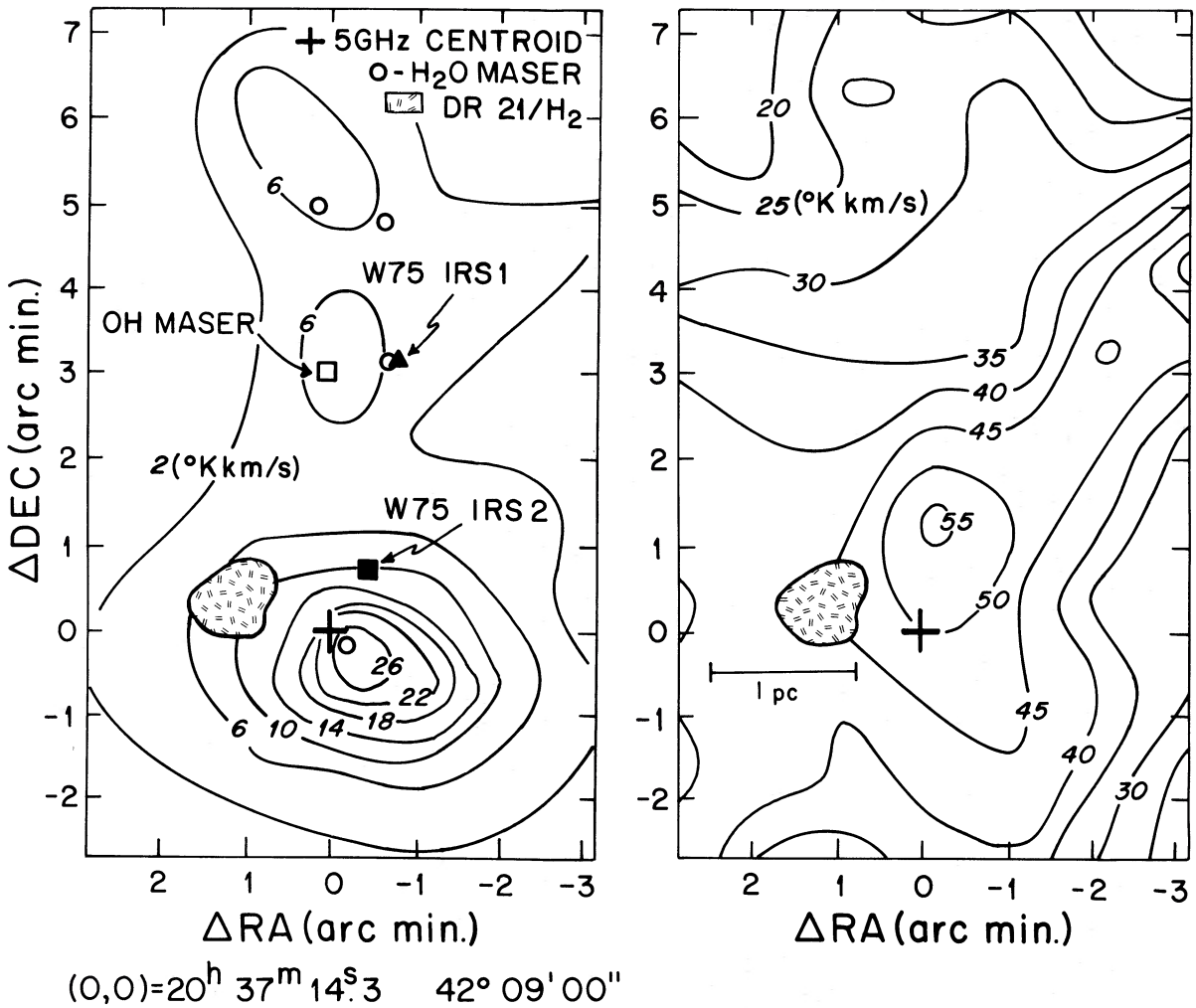

FIG. 3.—(*left*) Map of the integrated intensity [$\int_{-20}^{-10} T_A^*(^{12}CO)dv$] of the blue wing of the ^{12}CO emission in DR 21, based on data with 1′ spacing. The hatched area represents the H_2 emission region, contained within the half power contour of the $v = 1$–0 $S(1)$ line map of Fig. 1. The positions of the W75 infrared sources and the OH maser are from Wynn-Williams, Becklin, and Neugebauer (1974) and Wynn-Williams, Werner, and Wilson (1974), and the H_2O maser positions are from Habing and Israel (1979) and Genzel and Downes (1977). The zeroes of the right ascension and declination offsets are at the radio continuum emission centroid. (*right*) Map of the ^{12}CO intensity integrated between 5 and 20 km s^{-1}. This velocity interval includes the 9 km s^{-1} component associated with W75 N in addition to the red wing of the DR 21 −3 km s^{-1} component.

2′ west of IRS 1–3 which we do not confirm. The half-power extent of the H_2 $S(1)$ line emission (from Fischer *et al.* 1980) is indicated in Figure 7; this emission is located within the half-power contour of the ^{12}CO blue-wing emission and at the northern edge of the half-power contour of the red-wing emission. The measured angular diameter of the blue- and red-wing components are θ (FWHP) = 1.′15 and 1.′16 respectively. The blue-wing size reflects only the one-dimensional east-west FWHP size, since the continued velocity broadening to the south is part of the second outflow studied by Sanders (1984). We obtained a high-sensitivity ^{13}CO line profile at the (0, 0) position of the ^{12}CO map. The ratio of the ^{12}CO to ^{13}CO antenna temperatures R is plotted as a function of velocity in Figure 6. The average value of R in the blue and red wings is 23 ± 2 and 23 ± 5 respectively.

d) OMC-2

H_2 emission in the OMC-2 region is centered on IRS 4, the most luminous member of the cluster, and appears to be extended to the north about 15″ to 30″ (Fischer, Righini-Cohen, and Simon 1980; Thronson and Thompson 1982). Figure 8 shows that the ^{12}CO emission can be traced to at least ±6 km s^{-1} away from line center, and that this high-velocity emission is localized around IRS 4. Figure 9 shows that the blue- and red-wing emission peaks are separated by about 23″, which corresponds to 0.06 pc at a distance of 500 pc (Kutner, Evans, and Tucker 1976). The measured angular diameters of the blue- and red-wing emission regions are θ (FWHP) = 1.′75 and 1.′4. The ratio of the ^{12}CO to ^{13}CO antenna temperatures R is plotted for the OMC-2 IRS 4 position as a function of velocity in Figure 8. The average value of R in the blue and red wings is 26 ± 8 and 27 ± 7 respectively.

e) NGC 6334

An extended source of H_2 line emission is associated with the submillimeter Peak V region (see McBreene *et al.* 1979 for nomenclature convention in NGC 6334), and preliminary ^{12}CO observations showed that there is high-velocity flow within this molecular cloud (Fischer *et al.* 1982). We have obtained a high-sensitivity ^{12}CO map of the entire submillimeter Peak IV and V regions. The high-velocity CO emission peaks ~1′ west of and at the same declination as the H_2

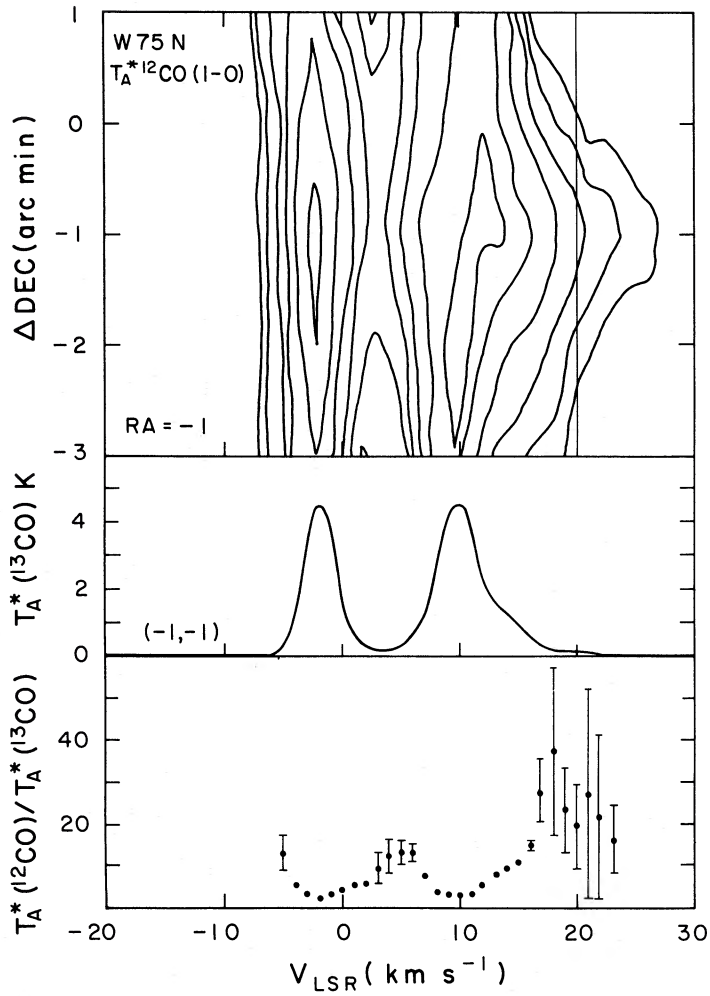

FIG. 4.—(*top*) Velocity-declination map of $T_A^*(^{12}CO)$ in the W75 N region. The data in this map were taken at 1′ spacing centered at the peak of the red-wing emission, i.e., at R.A.(1950) = $20^h36^m45^s.7$ (i.e., 1′ west of the H_2 peak) with the zero of declination offsets at the H_2 peak. The vertical line indicates the value taken for the velocity v_l. The contour levels are $T_A^* = 0.5$, 1, 2, 4, 8, and 12 K km s^{-1}. (*middle*) The ^{13}CO line profile and (*bottom*) the ratio $T_A^*(^{12}CO)/T_A^*(^{13}CO)$ are shown as a function of velocity for the central position of the velocity-declination map.

source (Fig. 10; see also Fig. 8 in Fischer *et al.* 1982). Figure 10 shows that blueshifted CO emission extends at least 18 km s^{-1} away from the line center and that the emission in the blue wing is stronger than in the red wing. The high-velocity flow in this molecular cloud appears to be very anisotropic. Both the blue and red wings are confused by other low-level emission components. A velocity component at +6 km s^{-1} interferes with the red-wing emission (see Fig. 10), and emission from the inner galactic disk underlies the entire blue wing. In our raw map of the integrated intensity of the antenna temperature between −13 and −25 km s^{-1}, the level of galactic-plane contamination was determined outside the region of the red wing. In addition to a possible but unknown constant intensity level, a linear gradient was apparent along the right-ascension direction. This gradient has been subtracted in the map presented in Figure 11 and in our calculations (§ IV*b*) in order to isolate the blueshifted high-velocity component. The quantity subtracted was $y = 2.5\Delta$ R.A. (arc minutes) +7.6 K km s^{-1}. The measured effective angular diameter of the blueshifted component is θ (FWHP) = 2′.

The ^{13}CO line profile and the ^{12}CO/^{13}CO line ratio at the peak of the H_2 *S*(1) line emission are shown in Figure 10. The average value of *R* in the blueshifted wing is 5.7 ± 0.5. We believe that this ratio is not intrinsic to the blue-wing emission but is confused by the same material along the line of sight that produced the gradient in the integrated intensities discussed above.

f) *Herbig-Haro Object 2*

Among the molecular hydrogen sources that we have detected and studied, the Herbig-Haro object 2 is the only one in which high-velocity wings were not apparent in the ^{12}CO line profile. The *S*(1) line emission was detected at the position of the Herbig-Haro object and is extended on a scale of ∼30″ (Fischer, Righini-Cohen, and Simon 1980; Elias 1980). Optical emission lines toward HH 2 show evidence for high-velocity material and shock excitation. Velocity dispersions of at least 110 km s^{-1} are present in the [O III] line profiles of HH 2 measured by Schwartz (1978), and comparison of relative optical-line intensities and theoretical models predict shock velocities of ∼110 km s^{-1} and preshock stellar-wind densities of ∼200 cm^{-3} (Schwartz 1978; Dopita 1978). A ^{12}CO line profile was obtained at the position of the Herbig-Haro object but the rms noise was 0.5 K. Our negative high-velocity CO result did not preclude the possibility that high-velocity molecular flows exist in this source. Such flows could exist at weaker

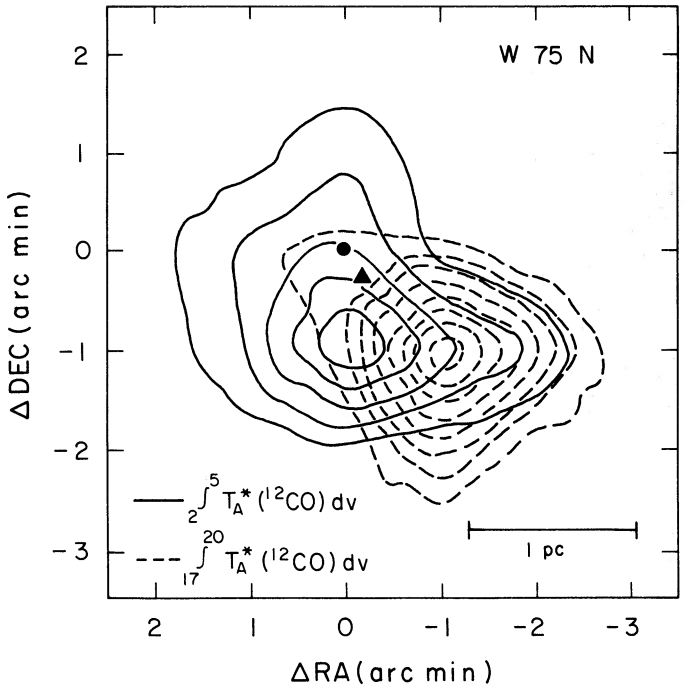

FIG. 5.—Map of the integrated intensity of the blue and red wings of the ^{12}CO emission in the W75 N region, based on data with 0.'75 spacing. The zeroes of the right ascension and declination offsets are at the position where H_2 emission was detected (Fischer, Righini-Cohen, and Simon 1980), R.A.(1950) = $20^h36^m51^s.1$, decl.(1950) = 42°27′20″. This is also the position of the H II region W75 N(A) (Haschick *et al.* 1981), marked with a filled circle. The position of the compact H II region W75 N(B) (Haschick *et al.*) is marked with a triangle. The contour levels are drawn at 3, 4, 5, ... K km s^{-1}.

levels than are detectable with the rms noise level obtained, or they could peak at a position that is displaced from the Herbig-Haro object itself. Recently, Edwards and Snell (1984) have detected high-velocity CO emission centered ~4′ north of HH 2 near V380 Ori. Red-wing emission at $v = 11$–18 km s^{-1} extends ~10′ to the south of V380 Ori, and HH 2 lies just inside the lowest plotted contour level of 2 K km s^{-1}. HH 2 itself does not seem to be a high-velocity source but rather appears to be caught up in outflowing gas from the star V380 Ori.

IV. ANALYSIS AND DISCUSSION

The observations reported here show that all the H_2 emission sources we have studied are closely associated with regions of high-velocity gas flow. We emphasize here that the flows are local, based on (1) their presence in all sources, (2) their proximity to the central star clusters, and (3) their small ($\lesssim 1'$) spatial extents (see spatial-velocity plots in Figs. 2, 4, 6, 8, and 10). In DR 21, as in the Orion molecular cloud (Solomon, Huguenin, and Scoville 1981), the H_2 emission region is clearly situated at the periphery of the high-velocity flow (Fig. 3). This suggests that the vibrationally excited H_2 has been heated by shocks as the outflowing gas interacts with the surrounding molecular cloud. Quantitatively, if it is true that for a given source the excited H_2 has been heated by shocks powered by the outflows, and if the energy outflow has been constant, then the energy in the flow must be sufficient to have driven the luminosity of the H_2 emission over the expansion lifetime of the source. Moreover, if the flow is driven radiatively by a star of luminosity L_*, the momentum transfer $\dot{p}$ from the radiation to the surrounding matter is limited by the constraint that

$$\dot{p} \leq \frac{L_* \tau_R}{c}, \tag{1}$$

where τ_R is the effective optical depth coupling the radiation to the surrounding material. It is possible to estimate mass, and hence the energy and momentum, in these flows from the ^{12}CO and ^{13}CO line data. The values of these quantities depend on the assumed excitation temperature and on the optical depth in the ^{12}CO and ^{13}CO lines. Our knowledge of these quantities is discussed in § IV*a*. The mass, momentum, and energy calculations are carried out in § IV*b*. We estimate the luminosity and total energy requirements of the molecular-hydrogen-line emission in § IV*c*. Finally, in § IV*d* we evaluate whether either the radiation pressure available from embedded infrared sources or the mechanical energy available from the expansion of the H II regions are sufficient to drive the high-velocity flows.

a) The Excitation Temperature, Optical Depth, and Clumpiness of the High-Velocity CO *Emission*

In the high-velocity-wing emission of DR 21, W75 N, NGC 7538, and OMC-2 (see Figs. 2, 4, 6, and 8), the observed ratio

$$R \equiv \frac{T_A^*(^{12}CO)}{T_A^*(^{13}CO)}$$

is $R \approx 25$, while in NGC 6334, $R = 5.7 \pm 0.5$. If the interstellar abundance ratio $\chi = {}^{12}CO/{}^{13}CO$ in these sources is taken to be equal to the solar ratio of 90 (consistent with ratios measured by Penzias 1983 and Scoville *et al.* 1983 in molecular clouds within 3 kpc of the Sun), the measured values of R in DR 21, W75 N, NGC 7538, and in OMC-2 suggest that $\tau(^{12}CO) > 1$ and $\tau(^{13}CO) < 1$. In the case of NGC 6334, where we believe that R is low due to emission from molecular-cloud material along the line of sight (see § III*e*), we adopt $R = 25$ as the intrinsic value of R. The optical depth $\tau(^{12}CO)$ can be obtained from the relation

$$R \approx \frac{1 - \exp[-\tau(^{12}CO)]}{1 - \exp[-\tau(^{13}CO)]} = \frac{1 - \exp[-\tau(^{12}CO)]}{1 - \exp[-\tau(^{12}CO)/\chi]} \tag{2}$$

if there are no fractionation effects and if $T_{ex}(^{12}CO) = T_{ex}(^{13}CO)$, where T_{ex} is the $J = 1$–0 excitation temperature. Thus for $R = 25$, $\tau \approx 3.6$. The values of τ derived in this manner are dependent on the assumed value of χ, which may vary due to effects such as stellar processing, fractionation, and selective dissociation. If the assumed accuracy of χ is 90 ± 40, $\tau = 3.6 \pm 2$ (for $R = 25$). Thus the conclusion that the $^{12}CO(J = 1$–$0)$ transition is optically thick for velocities where we have measured R seems firm, unless χ is very different in these flows from what it is in other molecular clouds. It is therefore surprising that although the sources appear to be spatially resolved, the antenna temperatures of the high-velocity emission in these sources are $T_A^*(^{12}CO) \leq 3$ K. This implies that either the $J = 0, 1$ levels are not thermalized or the lines are emitted in clumpy gas that does not uniformly fill the beam. Measurements of HCN and $H^{13}CN$ in the $J = 4$–3 transition by White, Avery, and Richardson (1984) and measurements of HCO^+ by Wootten *et al.* (1984) show that the high-velocity outflows in Orion and NGC 2071 have densities $\sim 10^5$–10^6. Thus in our analysis we assume that the lines are thermalized. We therefore carry out our analysis in terms of the filling factor f, the projected area filled by CO of optical depth

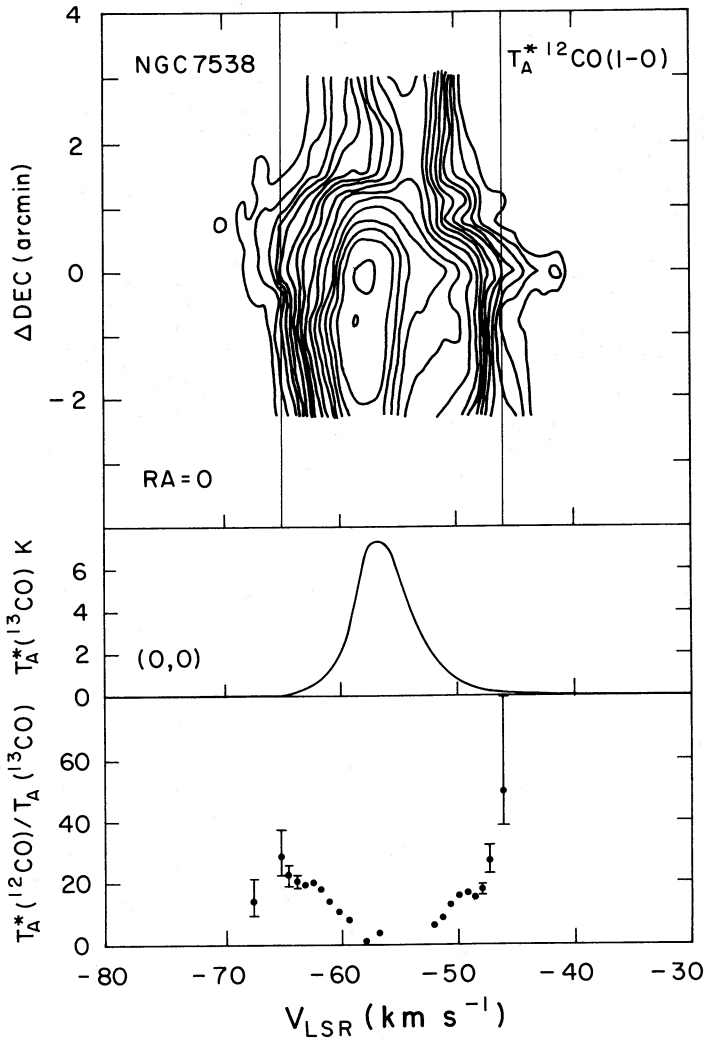

FIG. 6

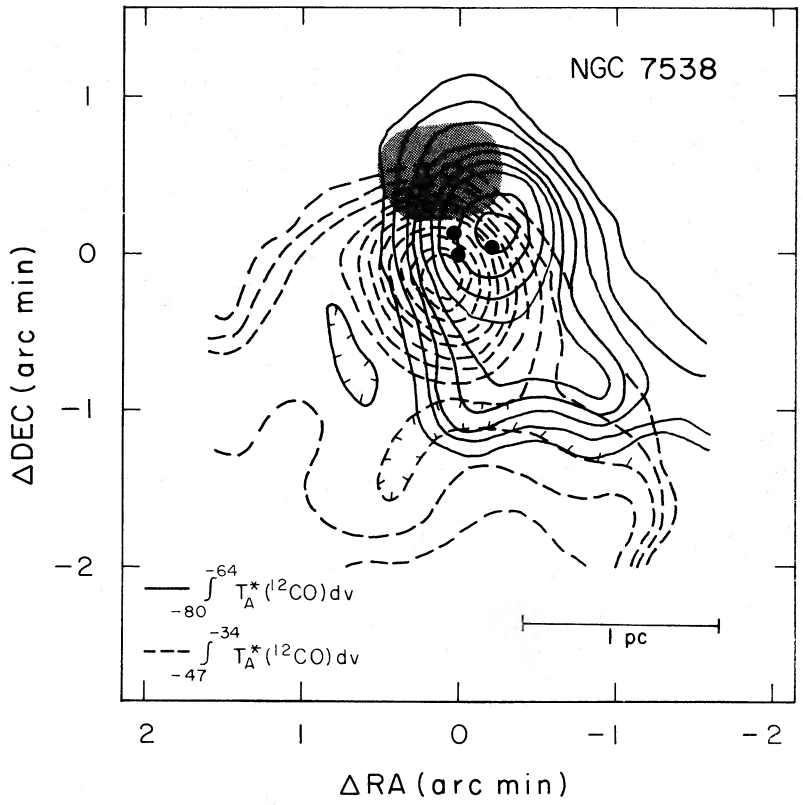

FIG. 7

FIG. 6.—(*top*) Velocity-declination map of $T_A^*(^{12}CO)$ in the NGC 7538 region. The (0, 0) position is at IRS 1, i.e., R.A.(1950) = $23^h11^m36^s.7$, decl.(1950) = 61°12′49″. The vertical lines indicate the values taken for the velocities v_l for the blue and red wings. The data were taken every half beam width (22″.5) between Δdecl. = −0.75, and +1.125 and every full beam width outside this range. The contour levels are T_A^* = 0.45, 0.9, 1.35, 1.8, 2.25, 3, 3.75, 4.5, 6, 7.5, 9, 10.5, 12, 13.5, 15, 18 K km s^{-1}. (*middle*) The ^{13}CO line profile and (*bottom*) the ratio $T_A^*(^{12}CO)/T_A^*(^{13}CO)$ as a function of velocity are shown at the position of IRS 1.

FIG. 7.—Map of the integrated intensity of the ^{12}CO emission of NGC 7538 in the blueshifted (*solid contours*) and the redshifted (*broken contours*) wing emission, based on data with 22″.5 spacing. The (0, 0) position of the map is at NGC 7538 IRS 1, R.A.(1950) = $23^h11^m36^s.7$, decl.(1950) = 61°11′48″. The shaded region marks the approximate half power extent of the H_2 $S(1)$ line emission region (Fischer *et al.* 1980). The positions of the compact H II regions IRS 1, 2, and 3 (Martin 1973) are marked by filled circles. The blue- and red-wing contour levels are drawn at 5, 6, 7, . . . K km s^{-1}.

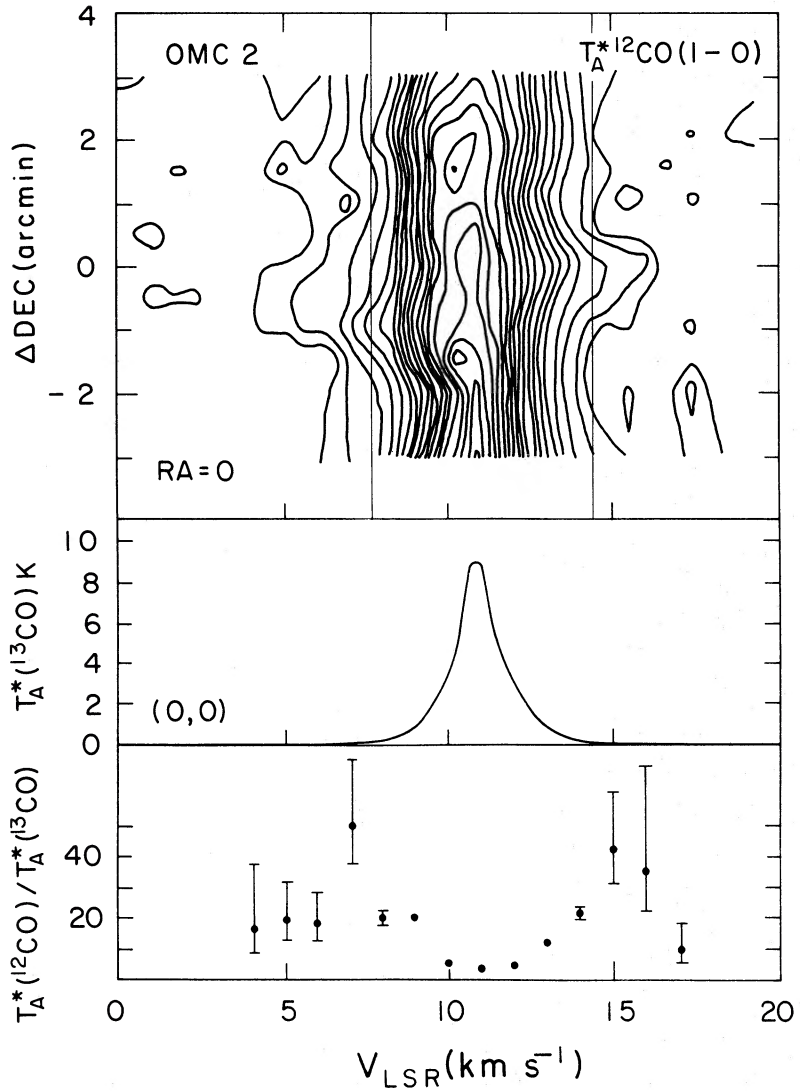

FIG. 8.—(*top*) Velocity-declination map of $T_A^*(^{12}CO)$ in the OMC-2 region. The maps are centered at the H_2 emission peak at IRS 4 (R.A.[1950] = $05^h32^m59^s.6$, decl.[1950] = $-05°11'32''$), and data were taken at 30″ spacing. The vertical lines indicate the values taken for v_l for the blue and red wings. The contour levels are drawn at 1.5, 2.5, ... 8.5 K km s^{-1}. (*middle*) The (^{13}CO) line profile and (*bottom*) the ratio $T_A^*(^{12}CO)/T_A^*(^{13}CO)$ as a function of velocity are shown at the position of IRS 4.

$\tau(^{12}CO)$ divided by the projected beam area;

$$f = \frac{T_A^*(^{12}CO)/\eta}{[5.5/(e^{5.5/T_{ex}} - 1) - 0.8][1 - e^{-\tau(^{12}CO)}]} . \quad (3)$$

The main beam coupling efficiency η is a slowly varying function of the source size for a particular antenna. We use $\eta = 0.56$ and $\eta = 0.66$ for the NRAO and FCRAO telescopes respectively, appropriate for source sizes of a few arc minutes. The optical depth $\tau(^{12}CO)$ is obtained from equation (2). Since the ratio R is found to be approximately constant over the extent of the high-velocity emission, the average value of R in the wings is used and $\tau(^{12}CO)$ is assumed to be constant.

Excitation temperatures have recently been measured in high-velocity wing sources by Snell *et al.* (1984). They find that the temperature of the high-velocity gas is close to the cloud-core temperature. We expect T_{ex} to be in the range 10–100 K, since this is the range of excitation temperatures normally deduced for molecular cloud cores. We adopt $T_{ex} = 25$ K in our calculations of the column density, mass, momentum, and energy and note that in the Raleigh-Jeans limit, where $kT_{ex} \gg h\nu$, these calculated quantities are proportional to the assumed value of T_{ex} in our analysis.

b) *The Mass, Momentum, and Energy Content of the High-Velocity Gas*

We calculate the column density of ^{12}CO molecules at the peak position of the high-velocity wing components using the expression

$$N_{peak}(^{12}CO) = 2.8 \times 10^{14}(T_{ex} + 1)(1 - e^{-5.5/T_{ex}})^{-1} \times \left[\tau(^{12}CO)\int_{|v_l - v_0|}^{|v_h - v_0|} f dv' + f(v_l)\tau(^{12}CO)|v_l - v_0|\right], \quad (4)$$

where $v' = |v - v_0|$ in km s^{-1}. Here the integral with respect to velocity is carried out from the highest velocity observed, v_h, to the lowest velocity from which emission is not observed at a position displaced from the high-velocity emitting region, v_l. This criterion was based approximately on the lowest contours plotted in Figures 2, 4, 6, 8, and 10. (The quantity v_l is indicated

TABLE 3

DERIVED PARAMETERS OF THE MOLECULAR FLOWS

Region (1)	Adopted Distance (kpc) (2)	$\tau(^{12}CO)$ (3)	t_e (10^4 yr) (4)	$N_{peak}(H_2)$ (10^{21} cm^{-2}) (5)	M_{hv} ($M_\odot$) (6)	P_{hv} (10^{41} g cm s^{-1}) (7)	E_{hv} (10^{46} ergs) (8)	$L(H_2)t_e$ (10^{46} ergs) (9)	$L_* t_e$ (10^{50} ergs) (10)	$L_* t_e/c$ (10^{41} g cm s^{-1}) (11)
DR 21[a,b]	2[c]	3.5	2.0	13	170	2.4	14	2.3	1.6[d]	0.05
W75 N[a,b]	2[c]	3.7	2.3	12	130	1.9	10	0.12	1.2[d]	0.04
NGC 7538[b]	2.8[e]	3.9	2.6	7.0	44	0.55	2.3	2.1	5.2[f]	0.17
OMC-2	0.5[g]	3.3	0.9	4.5	1.8	0.013	0.033	0.011	0.39[h]	0.013
NGC 6334[a]	1.7[i]	...	1.3	11	86	1.0	4.1	0.52	2.6[j]	0.09

[a] Only one wing (blue- or redshifted) was used to calculate derived parameters due to confusion from line-of-sight emission. The tabulated quantities N_{peak}, M_{hv}, P_{hv}, and E_{hv} were obtained by doubling calculated values for a single wing.

[b] Luminosities $L(H_2)$ and L_* from references adopting distances differing from those in this work were adjusted for this discrepancy.

[c] See text.

[d] Harvey, Campbell, and Hoffmann 1977.

[e] Crampton, Georgelin, and Georgelin 1978.

[f] Werner *et al.* 1979.

[g] Kutner, Evans, and Tucker 1976; Genzel *et al.* 1981.

[h] Smith *et al.* 1979.

[i] Neckel 1978.

[j] McBreene *et al.* 1979.

for the sources studied in this work in Figs. 2, 4, 6, 8, and 10; v_l and v_h are tabulated in Table 2.) The integral is then continued with $f(v) = f(v_l)$ until $v = v_0$, the central velocity of the cloud. In the sources studied here, this latter part of the integral contributes a mean fractional value of 0.66 ± 0.11 to the integral.

To calculate the mass, momentum, and energy in the high-velocity gas, the extent of the source d_{hv} is determined by deconvolving the antenna beam according to

$$d_{hv} = D[\theta\,(\mathrm{FWHP})^2 - \theta_{\mathrm{beam}}^2]^{1/2}\,,$$

where D is the assumed distance to the source, θ (FWHP) is the measured source size, and θ_{beam} is the antenna main beam. The total mass, radial momentum, and energy are then given by

$$M_{hv} = \xi(^{12}\mathrm{CO})^{-1} m(\mathrm{H_2}) N_{\mathrm{peak}}\, \pi(d_{hv}/2)^2\,, \quad (5)$$

$$P_{hv} = \xi(^{12}\mathrm{CO})^{-1} m(\mathrm{H_2}) N'_{\mathrm{peak}}\, \pi(d_{hv}/2)^2\,, \quad (6)$$

$$E_{hv} = \tfrac{1}{2}\xi(^{12}\mathrm{CO})^{-1} m(\mathrm{H_2}) N''_{\mathrm{peak}}\, \pi(d_{hv}/2)^2\,, \quad (7)$$

where $m(H_2)$ is the mass of the H_2 molecule. $\xi(^{12}CO)$, the interstellar abundance of ^{12}CO relative to H_2, is taken to be $\xi(^{13}CO) \times \chi$, where $\xi(^{13}CO) = 1 \times 10^{-6}$ (Sanders, Solomon, and Scoville 1984). N' and N'' are the first and second moments of equation (4) with respect to $|v - v_0|$. The mean fractional portion of N' and N'' contributed by the integration between v_0 and v_l (where T_A^* was assumed to be constant) was 0.41 ± 0.18 and 0.26 ± 0.20 respectively. For the sources in which emission from one of the wings was contaminated by emission from other velocity components, i.e., DR 21—blue, W75 N—red, and NGC 6334—blue, only the uncontaminated wing component was used in these calculations. The results were then doubled to account for the contaminated wing. The calculated values of the quantities N_{peak}, M_{hv}, P_{hv}, and E_{hv} are given in columns (5)–(8) of Table 3. Since the values of M_{hv}, P_{hv}, and E_{hv} are proportional to D^2, these quantities are uncertain due to the uncertainty in the adopted distances (tabulated in col. [2] of Table 3) to these sources. All parameters [$f(v)$, $M(v)$, $P(v)$, and $E(v)$] are strong functions of the velocity, $|v - v_0|$. Of particular interest are the variations of the filling factor and the mass as a function of the velocity in these sources. Typically, $T_A^*(v_l) \approx 1$–5 K and $T_A^*(v_h) \approx 0.1$–0.5 K, where $|v_l - v_0| \approx 3$–11 and $|v_h - v_0| \approx 10$–30. Thus it can be seen from equations (3), (4), and (5) that $f(v_l) \approx 10\%$–50% and $f(v_h) \approx 1\%$–5%, and

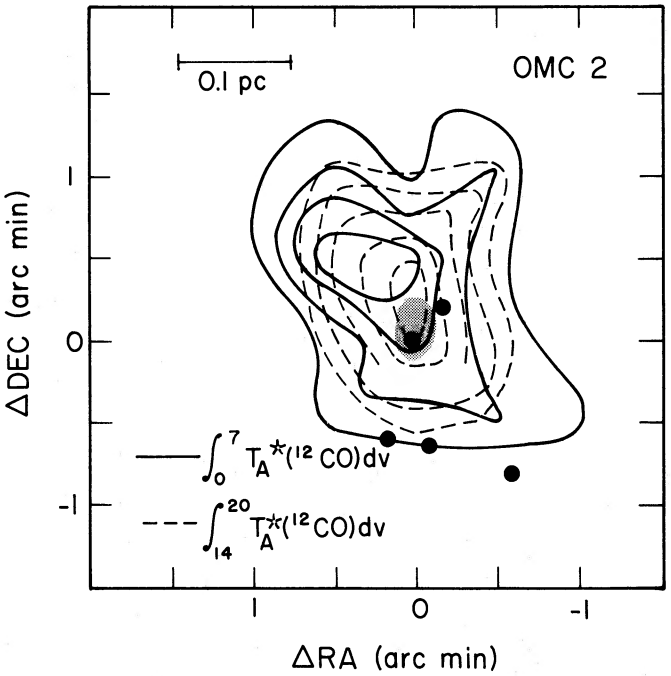

FIG. 9.—Map of the integrated intensity of the ^{12}CO emission of OMC-2 in the blueshifted (*solid contours*) and the redshifted (*broken contours*) wing emission. The (0, 0) position of the map is at OMC-2 IRS 4, R.A.(1950) = $5^h32^m59^s6$, decl.(1950) = $-5°11'32''$. The shaded region marks the approximate extent of the H_2 $S(1)$ line-emission region (Fischer, Righini-Cohen, and Simon 1980). The positions of IRS 1, 2, 3, 4, and 5 (Gatley *et al.* 1974) are marked by filled circles. The contour levels are drawn at 3.5, 4.5, 5.5, 6.5, and 7.5 K km s^{-1}.

Mdv decreases by a factor of 10 between v_l and v_h. If τ is constant over this velocity range, as we have assumed, this implies that high-velocity clumps must have higher densities than low-velocity clumps (for spherical clumps). This seems rather ad hoc and may be indicative that the optical depth is *not* constant over the entire velocity range.

c) *The Relationship of the High-Velocity Flows and the Regions of Shocked Gas*

In this section we compare the energy observed in the high-velocity gas to the energy radiated by the vibrationally excited

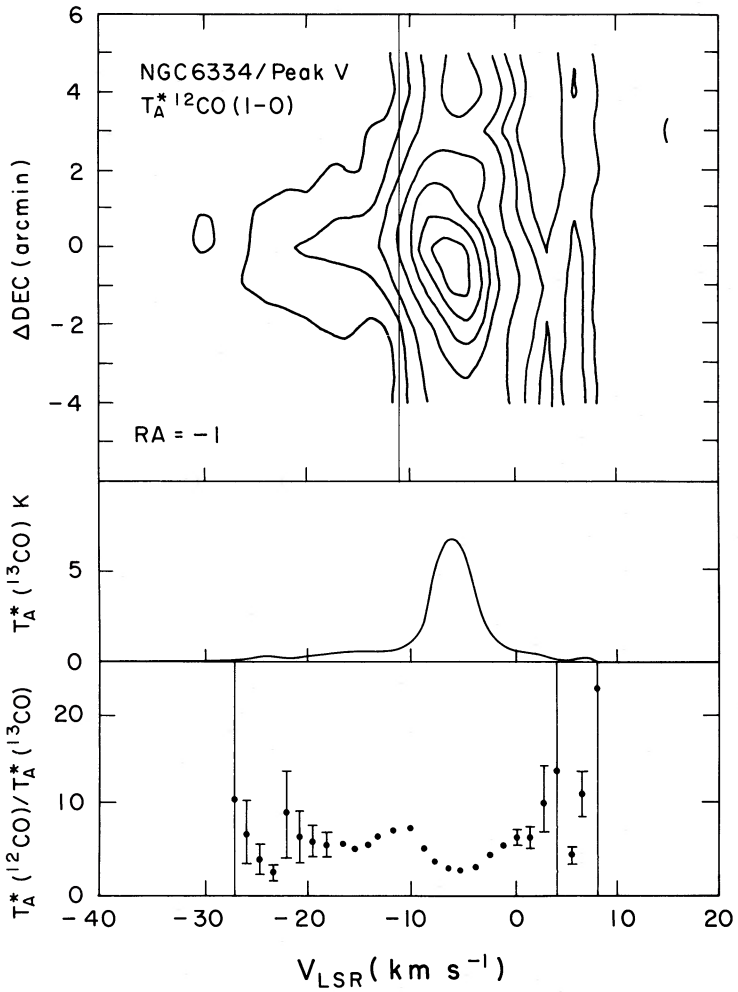

FIG. 10.—(*top*) Velocity-declination map of $T_A^*(^{12}CO)$ in the NGC 6334/Peak V region. The data in this map were taken at 1′ spacing centered at the peak of the blue-wing emission, i.e., at R.A.(1950) = $17^h16^m34^s.3$ (1′ west of the H_2 emission peak), with the zero of the declination coordinates at decl.(1950) = −35°54′49″ (at the H_2 emission peak). The vertical line indicates the value taken for v_l. The contour levels are drawn at 1, 2, 4, 8, 16, 20, and 24 K km s^{-1}. (*middle*) The ^{13}CO line profile, and (*bottom*) the ratio $T_A^*(^{12}CO)/T_A^*(^{13}CO)$ as a function of velocity are shown at the central position of the velocity declination map, i.e. Δdecl. = 0.

H_2 over the lifetime of the flow. This is a quantitative test of the model in which the ^{12}CO high-velocity wing emission is a tracer of the post-shock gas behind the H_2 cooling region.

We assume that the high-velocity gas flows are due to expansion. For example, in DR 21, it is unlikely that the gas is gravitationally bound because of the large central mass implied by $M \geq v^2 r/2G \approx 7 \times 10^4\ M_\odot$. Since this is on the order of the mass of the entire cloud (Dickel, Dickel, and Wilson 1978), pure rotation and collapse can be ruled out. The flows studied here are anisotropic, i.e., generally the red- and the blue-wing emission regions peak at different positions and they are somewhat elongated in projection. Since their separations are typically smaller than their extents, we estimate their expansion times using their average extents d_{hv} and their observed highest outflow velocities $v_{hv} \equiv |v_h - v_0|$. Assuming their outflow velocities have been constant over most of their lifetimes, we obtain expansion times $t_e \approx 0.5 d_{hv}/v_{hv}$ in the range 1–3 × 10^4 yr and list them in column (4) of Table 3. (In sources where both blue and red wings were studied, the average value of t_e was used).

As pointed out by Beckwith (1980), if the H_2 vibrational radiation accounts for most of the postshock cooling in an isothermal shock, then the rate at which energy is radiated in these lines is expected to be about equal to the rate at which bulk kinetic energy is deposited into the gas (see Appendix). Thus, assuming constant outflow velocities, we expect that $E_{hv} \approx L(H_2)t_e$, where $L(H_2)$ is the luminosity in all the molecular-hydrogen cooling lines. Temperatures between 1500 K and 3000 K have been measured in a number of molecular-hydrogen emission regions (Orion—Beckwith, Persson, and Neugebauer 1979; Scoville *et al.* 1982; Knacke and Young 1981; Davis, Larson, and Smith 1982; DR 21—Fischer 1981; OMC-2—Thronson and Thompson 1982). Therefore we estimate $L(H_2)$ from the measurements of Fischer, Righini-Cohen, and Simon (1980), Fischer *et al.* (1980), and Fischer *et al.* (1982) by assuming a rotation-vibration temperature $T_{r-v} \approx 2{,}000$ K. We list the estimated values of $L(H_2)t_e$ in column (9) of Table 3. These estimates neglect extinction. The calculated values of the ratio $L(H_2) \cdot t_e/E_{hv}$ are plotted in Figure 12 for the sources studied in this work. The values of this ratio are in the range 10^{-2} to 0.9. (The low value of 10^{-2} is for W75 N, where the H_2

emission was not fully mapped.) There were many assumptions involved in the calculation of this ratio. Extinction was neglected in the calculation of $L(H_2)$, and velocity projection effects were ignored in the calculation of E_{hv}. In addition, the highest velocities present in the outflows may not have been detected due to sensitivity limitations. We also note that some of the high-velocity gas may be atomic and that some shocked H_2 may be dissociated. It may also be that the $^{13}CO/H_2$ ratio is higher than we assumed, if, for example all the C is tied up in CO in regions where the dust temperature is 50 K or higher, as suggested by Scoville *et al.* (1983). With these caveats, we marvel that this ratio is $\lesssim 1$ and we view this as strong evidence that the high-velocity gas *does* power the H_2 emission.

d) Driving Mechanisms

Analysis of the observations reported here has demonstrated that these high-velocity flows are the result of gas *outflows* powered by one or more young stellar objects associated with the central star clusters. If temporally constant, these outflows appear to have the energy available to drive the hot, shocked gas that emits the 2 μm H_2 lines. What is the mechanism by which these young stellar objects power the outflows themselves? We consider four general categories of driving mechanisms: (1) radiation pressure, (2) H II region expansion, (3) nonradiatively driven stellar winds, and (4) mini-explosions. We will show that the first two categories are unlikely to power the outflows studied here.

The energy and momentum that are available from radiation pressure can be estimated from the total measured infrared fluxes and the adopted distance to these sources. Values of $L_* t_e$ and $L_* t_e/c$ are tabulated in columns (10) and (11) of Table 3, where L_* is the total infrared luminosity. Energetically, radiation pressure can power the flow since the mechanical energy of these outflows E_{hv} is a small fraction of the total luminous energy $L_* t_e$. This fraction varies from 10^{-3} for DR 21 to 10^{-5} for OMC-2. From the constraint that momentum transfer from the radiation to the surrounding matter is limited by equation (1), we derive effective optical depths $\tau_R \approx 1$–50 (see Fig. 13). For comparison Solomon, Huguenin, and Scoville (1981) and Bally and Lada (1983) find $\tau_R > 100$ for other high-velocity flows. It should be noted that they used the approximation $P_{hv} = MV$, where V is a characteristic velocity which is close to the largest observed velocity. In the present work equation (6) was used [i.e., $P_{hv} = \int M(v)vdv$, where v is the observed line-of-sight velocity], and lower values of τ_R were derived.

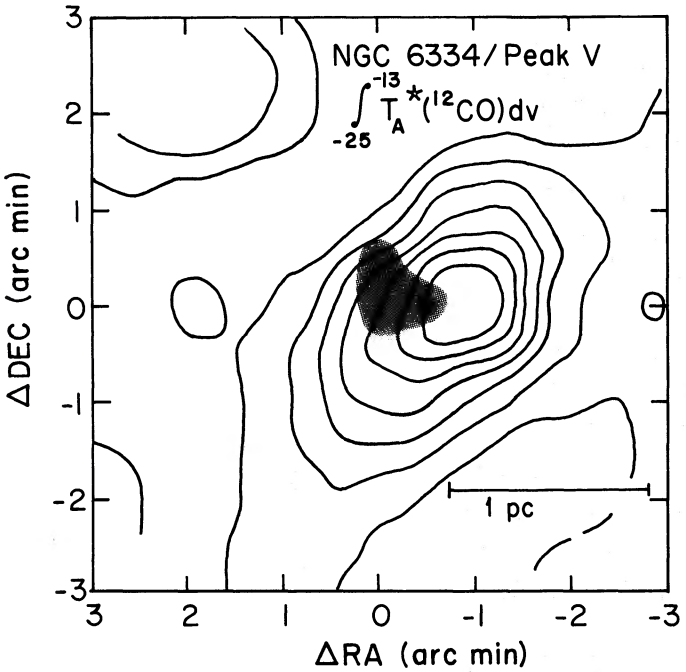

FIG. 11.—Map of the integrated intensity of the blue wing of the ^{12}CO emission of NGC 6334 in the Peak V region. A linear gradient of integrated intensity along the right-ascension direction was subtracted from the data for clarity (see text). The (0, 0) position of the map is at the H_2 position. The shaded region marks the half-power extent of the H_2 $S(1)$ line-emission region (Fischer *et al.* 1982). The Peak V near-infrared source (Fischer *et al.* 1982) is marked with a filled circle. The contour levels are drawn at 9, 12, 15, 18, 21, 24, and 27 K km s^{-1}.

For OMC-2 and NGC 7538, $\tau_R = 1$ and 3 respectively. Thus radiation pressure could conceivably be a viable accelerating mechanism in these objects. However, the values of τ_R derived for DR 21 and W75 N are difficult to reconcile with near-infrared optical depths that are inferred from recombination-line decrements. As Solomon, Huguenin, and Scoville (1981) show, it is at near-infrared wavelengths at which most of the scattering is expected to occur. At shorter wavelengths, scattering is accompanied by absorption and infrared emission. Yet from the Bα/Bγ ratios measured in DR 21 and W75 N (Righini-Cohen, Simon, and Young 1979), $A(4\ \mu m) \approx 0.04\ A_v < 5$. Thus it appears unlikely that radiation pressure drives the flows. If radiation pressure does indeed power the outflows in these objects, either (1) the scattering occurs at optical or UV wavelengths due to high-albedo grains, (2) the extinction derived from the recombination lines is in error, or (3) the objects that power the flows are so highly obscured that they have not been identified.

The possibility that H II region expansion due to the high pressure in the hot ionized gas could cause the high-velocity flows and subsequent shock heating should be examined. Compact H II regions are present near the centers of the outflows in DR 21, W75 N, and NGC 7538, while upper limits exist on the amount of compact ionized gas present in OMC-2 and NGC 6334/Peak V (Fischer 1981; Thronson and Thompson 1982; Rodríguez, Cantó, and Moran 1982). The widths of the H109a and Bα recombination lines in DR 21, for example, are $\Delta v \approx 44$ km s^{-1} (Mezger *et al.* 1967; Roelfsema, private communication), implying supersonic flows. Thermal expansion of the *compact* H II regions near the centers of the outflows in DR 21, W75 N, and NGC 7538 cannot be responsible for the outflows because the observed spatial extent of the ionized gas is much smaller than the extent of the high-velocity flow regions. However, the *extended* envelopes of these compact H II regions, such as the faint extension of the DR 21 H II region reported by Ryle and Downes (1967) and Wynn-Williams (1971), may trace the flow that is responsible for driving the high-velocity molecular flows. Since high-resolution radio interferometry is insensitive to large-scale structures, only low-spatial-resolution radio maps would accurately measure ionized flows large enough to drive these molecular flows. High-sensitivity, low-spatial-resolution radio-continuum studies could provide information about the density and structure of such envelopes, while velocity-resolved recombination-line measurements would reveal the velocity of expansion.

Based on these arguments we believe that either (1) nonradiatively driven stellar winds or (2) mini-explosions related to the star-formation process are responsible for the outflows

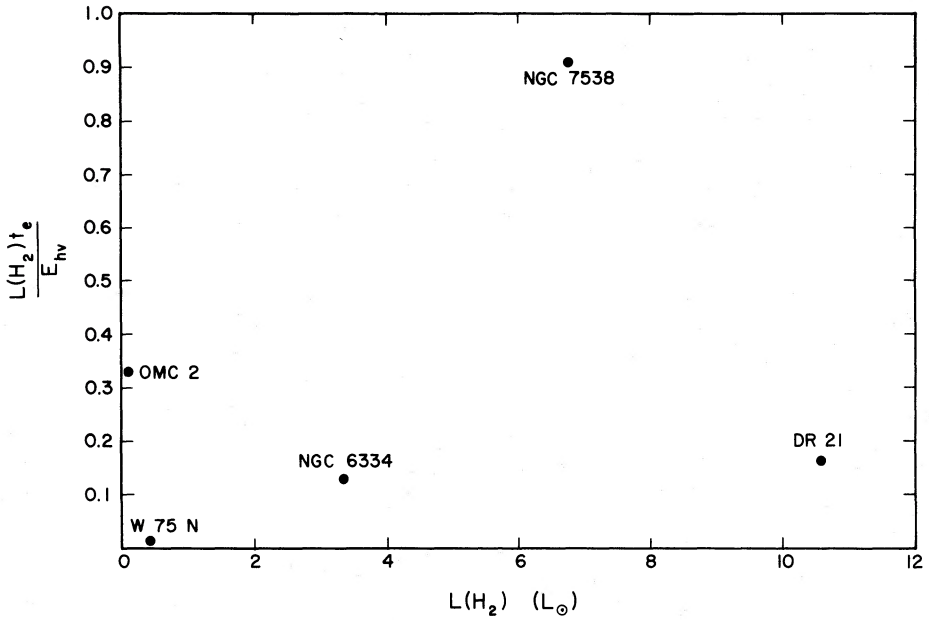

FIG. 12.—The ratio $L(H_2)t_e/E_{hv}$ versus $L(H_2)$. The values of $L(H_2)$ are taken from Fischer, Righini-Cohen, and Simon (1980) and Fischer *et al.* (1980, 1982); (adjusted for differences in adopted distances), and no correction for extinction was made.

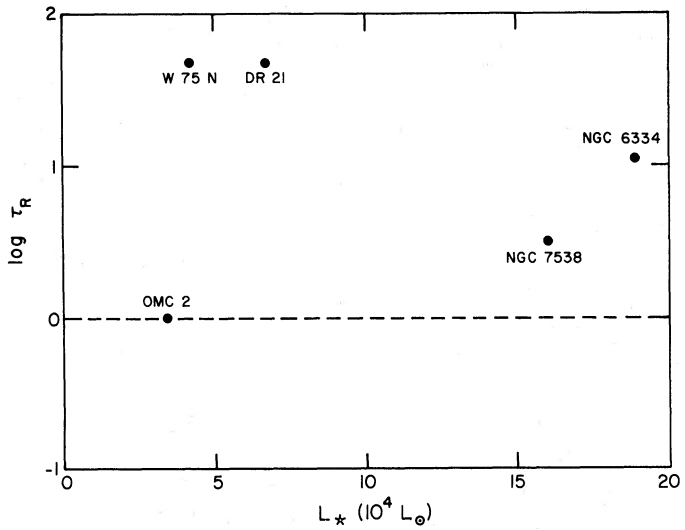

FIG. 13.—The ratio $\tau_R = (P_{hv}/t_e)/(L_*/c)$ vs. L_*

discussed here. Millimeter-wave interferometric measurements of the molecular flows studied here would provide a view of the spatial-velocity structure within these flows that could help chose between these possibilities.

IV. CONCLUSIONS AND SUMMARY

Our major conclusions can be summarized as follows:

1. The main result of this study is the discovery of low-level, highly localized ($\sim 1'$–$2'$), anisotropic molecular flows with velocities 10 km s^{-1} < v_{hv} < 30 km s^{-1} associated with the H_2 2 μm emission regions. In the case of DR 21, the H_2 region peaks at the periphery of the integrated CO(J = 1–0) distribution. In other cases, the H_2 emission peaks within the localized molecular flows traced by the CO emission, as expected for bipolar flows with randomly oriented axes. Thus it appears that bipolar outflows are a common phenomenon in young stellar objects.

2. The optical depth in the ^{12}CO(J = 1–0) line in these flows is moderate, $\tau < 4$. The molecular gas appears to be clumpy.

3. Comparison of the energy observed in the high-velocity gas with the energy radiated by the vibrationally excited H_2 over the lifetime of the flow yields values of the ratio $L(H_2)t_e/E_{hv}$ in the range 0.01–0.9. Allowing for the uncertainties in the calculations including our ignorance of the extinction to the H_2 regions, the fact that this ratio is $\lesssim 1$ is strong evidence that the H_2 emission is shock-excited and that the molecular flows do drive the H_2 emission regions.

4. The spatial extents of the flow regions are in the range 0.25–1 pc. The derived expansion times are in the range 1–3 × 10^4 yr.

5. The mechanical energy of these outflows is a small fraction of the total luminous energy of the embedded sources. This fraction ranges from 10^{-3} to 10^{-5} for these sources.

6. We find that both radiation pressure and H II region expansion are unlikely to be the driving mechanism of most of these high-velocity molecular flows.

We would like to acknowledge the contributions of Giovanna Righini-Cohen for her participation in the acquisition of the high-resolution map of the DR 21 H_2 region and of Jim Barrett for his help in obtaining some of the ^{12}CO data. We also thank Dick Joyce for technical assistance with the CVF spectrometer. This research was supported in part by NSF grant 8116049.

APPENDIX

Here we give a simple argument to show that isothermal shocks radiate energy at about the same rate as they deposit bulk kinetic energy in a flow (as pointed out by Beckwith 1980 in a similar context).

In the reference frame of the shock, the total specific energy (energy per unit mass) in the preshock gas is

$$e_0 = \tfrac{1}{2}u_0^2 + (\gamma/\gamma - 1)p_0/\rho_0 ,$$

where u, p, ρ, and γ are the velocity, pressure, density, and ratio of specific heats of the gas. In the postshock region,

$$e_2 = \tfrac{1}{2}u_2^2 + (\gamma/\gamma - 1)p_2/\rho_2 .$$

The subscripts "0" and "2" denote the preshock region and the radiatively cooled postshock region respectively. For an isothermal shock,

$$(\gamma/\gamma - 1)p_0/\rho_0 \approx (\gamma/\gamma - 1)p_2/\rho_2 .$$

Therefore the energy radiation by the shock is

$$e_0 - e_2 \approx \frac{1}{2}\, v_s^2 - \frac{1}{2}\,\frac{v_s^2}{M_0^2} \approx \frac{1}{2}\, v_s^2 ,$$

where v_s is the shock velocity and $M_0 \gg 1$ is the Mach number in the preshock gas. This is about equal to the specific kinetic energy deposited in the postshock gas ($\approx \frac{1}{2}v_s^2$) in the *rest* frame of reference.

REFERENCES

Bally, J., and Lada, C. J. 1983, *Ap. J.*, **265**, 824.
Bally, J., and Lane, A. 1982, *Ap. J.*, **257**, 612.
Beckwith, S. 1980, in *IAU Symp. 96, Infrared Astronomy*, ed. C. G. Wynn-Williams and D. P. Cruikshank (Dordrecht: Reidel), p. 167.
Beckwith, S., Persson, S. E., and Neugebauer, G. 1979, *Ap. J.*, **227**, 436.
Campbell, B., and Thompson, R. I. 1984, *Ap. J.*, **279**, 650.
Cong, H. I. 1977, Ph.D. thesis, Columbia University.
Crampton, D., Georgelin, Y. M., and Georgelin, Y. P. 1978, *Astr. Ap.*, **66**, 1.
Davis, D. S., Larson, H. P., and Smith, H. A. 1982, *Ap. J.*, **259**, 166.
Dickel, J. R., Dickel, H. R., and Wilson, W. J. 1978, *Ap. J.*, **223**, 840.
Dopita, M. A. 1978, *Ap. J. Suppl.*, **37**, 117.
Edwards, S., and Snell, R. L. 1984, *Ap. J.*, **281**, 237.
Elias, J. H. 1980, *Ap. J.*, **241**, 728.
Fischer, J. 1981, Ph.D. thesis, State University of New York at Stony Brook.
Fischer, J., Joyce, R. R., Simon, M., and Simon, T. 1982, *Ap. J.*, **258**, 165.
Fischer, J., Righini-Cohen, G., and Simon, M. 1980, *Ap. J. (Letters)*, **238**, L155.
Fischer, J., Righini-Cohen, G., Simon, M., Joyce, R. R., and Simon, T. 1980, *Ap. J. (Letters)*, **240**, L95.
Gatley, I., Becklin, E. E., Matthews, K., Neugebauer, G., Penston, M. V., and Scoville, N. 1974, *Ap. J. (Letters)*, **191**, L121.
Gautier, T. N., III. 1978, Ph.D. thesis, University of Arizona.
Gautier, T. N., III, Fink, U., Treffers, R. R., and Larson, H. P. 1976, *Ap. J. (Letters)*, **207**, L129.
Genzel, R., and Downes, D. 1977, *Astr. Ap.*, **61**, 117.
Genzel, R., Reid, M. J., Moran, J. M., and Downes, D. 1981, *Ap. J.*, **244**, 844.
Habing, H. J., and Israel, F. P. 1979, *Ann. Rev. Astr. Ap.*, **17**, 345.
Harris, S. 1973, *M.N.R.A.S.*, **162**, 5P.
Harvey, P. M., Campbell, M. F., and Hoffmann, W. F. 1977, *Ap. J.*, **211**, 786.
Haschick, A. D., Reid, M. J., Burke, B. F., Moran, J. M., and Miller, G. 1981, *Ap. J.*, **244**, 76.
Knacke, R. F., and Young, E. T. 1981, *Ap. J. (Letters)*, **249**, L65.
Kutner, M. L., Evans, N. J., II, and Tucker, K. D. 1976, *Ap. J.*, **209**, 452.
Lada, C. J., and Harvey, P. M. 1981, *Ap. J.*, **245**, 58.
Martin, A. H. M. 1973, *M.N.R.A.S.*, **163**, 141.
McBreene, B., Fazio, G. G., Stier, M., and Wright, E. L. 1979, *Ap. J.*, **232**, L183.
Mezger, P. G., Altenhoff, W., Schraml, J., Burke, B. F., Riefenstein, E. C. III, and Wilson, T. L. 1967, *Ap. J. (Letters)*, **150**, L157.
Nadeau, D., Geballe, T. R., and Neugebauer, G. 1982, *Ap. J.*, **253**, 154.
Neckel, T. 1978, *Astr. Ap.*, **69**, 51.
Penzias, A. A. 1983, *Ap. J.*, **273**, 195.
Persson, E., Geballe, T. R., Simon, T., Lonsdale, C. J., and Baas, F. 1981, *Ap. J. (Letters)*, **251**, L85.
Righini-Cohen, G., Simon, M., and Young, E. T. 1979, *Ap. J.*, **232**, 782.
Rodríguez, L. F., Cantó, J., and Moran, J. M. 1982, *Ap. J.*, **255**, 103.
Ryle, M., and Downes, D. 1967, *Ap. J. (Letters)*, **148**, L17.
Sanders, D. B. 1985, in preparation.
Sanders, D. B., Solomon, P. M., and Scoville, N. Z. 1984, *Ap. J.*, **276**, 182.
Schwartz, R. D. 1978, *Ap. J.*, **223**, 884.
Scoville, N. Z., Hall, D. N. B., Kleinmann, S. G., and Ridgway, S. T. 1982, *Ap. J.*, **253**, 136.
Scoville, N., Kleinmann, S. G., Hall, D. N. B., and Ridgway, S. T. 1983, *Ap. J.*, **275**, 201.
Shull, J. M. and Beckwith, S. 1982, *Ann. Rev. Astr. Ap.*, **20**, 163.
Simon, T., and Joyce, R. R. 1983, *Ap. J.*, **265**, 864.
Smith, J., Lynch, D. K., Cudaback, D., and Werner, M. W. 1979, *Ap. J.*, **234**, 902.
Snell, R. L., Scoville, N. Z., Sanders, D. B., and Erickson, N. R. 1984, *Ap. J.*, **284**, 176.
Solomon, P. M., Huguenin, G. R., and Scoville, N. Z. 1981, *Ap. J. (Letters)*, **245**, L19.
Thronson, H. A., and Thompson, R. I. 1982, *Ap. J.*, **254**, 543.
Werner, M. W., Becklin, E. E., Gatley, I., Matthews, K., Neugebauer, G., and Wynn-Williams, C. G. 1979, *M.N.R.A.S.*, **188**, 463.
White, G. J., Avery, L. W., and Richardson, K. J. 1984, preprint.
Wooten, A., Loren, R. B., Sandqvist, A., Friberg, P., and Hjalmarson, A. 1984, *Ap. J.*, **279**, 633.
Wynn-Williams, C. G. 1971, *M.N.R.A.S.*, **151**, 41.
Wynn-Williams, C. G., Becklin, E. E., and Neugebauer, G. 1974, *Ap. J.*, **187**, 473.
Wynn-Williams, C. G., Werner, M. W., and Wilson, W. J. 1974, *Ap. J.*, **187**, 41.

JACQUELINE FISCHER: E. O. Hulburt Center for Space Research, Naval Research Laboratory, Code 4138F, Washington, DC 20375

DAVID B. SANDERS: Downes Lab., 320-47, Caltech, Pasadena, CA 91125

MICHAL SIMON and PHILLIP SOLOMON: Astronomy Program, Department of Earth and Space Sciences, State University of New York, Stony Brook, NY 11794